

# Nanoscale Electrochemical Phenomena of Polarization Switching in Ferroelectrics

Anton V. Ievlev,<sup>\*,†,‡,§,ID</sup> Chance C. Brown,<sup>†,§</sup> Joshua C. Agar,<sup>||</sup> Gabriel A. Velarde,<sup>||</sup> Lane W. Martin,<sup>||,ID</sup> Alex Belianinov,<sup>†,‡,ID</sup> Petro Maksymovych,<sup>†,‡</sup> Sergei V. Kalinin,<sup>†,‡,ID</sup> and Olga S. Ovchinnikova<sup>\*,†,‡,ID</sup>

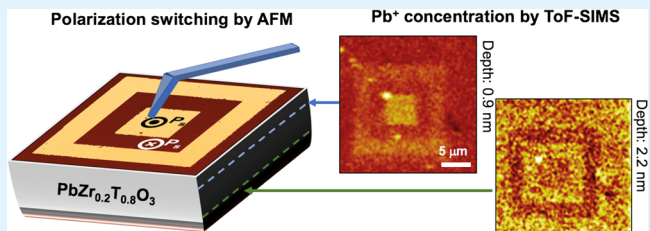
<sup>†</sup>The Center for Nanophase Materials Sciences and <sup>‡</sup>Institute for Functional Imaging of Materials, Oak Ridge National Laboratory, 1 Bethel Valley Rd., Oak Ridge, Tennessee 37831, United States

<sup>§</sup>The Bredesen Center, University of Tennessee, 821 Volunteer Blvd, Knoxville, Tennessee 37920 United States

<sup>||</sup>Department of Materials Science and Engineering, University of California Berkeley, Berkeley, California 94720, United States

## Supporting Information

**ABSTRACT:** Polarization switching is a fundamental feature of ferroelectric materials, enabling a plethora of applications and captivating the attention of the scientific community for over half a century. Many previous studies considered ferroelectric switching as a purely physical process, whereas polarization is fully controlled by the superposition of electric fields. However, screening charge is required for thermodynamic stability of the single domain state that is of interest in many technological applications. The screening process has always been assumed to be fast; thus, the rate-limiting phenomena were believed to be domain nucleation and domain wall dynamics. In this manuscript, we demonstrate that polarization switching under an atomic force microscopy tip leads to reversible ionic motion in the top 3 nm of  $\text{PbZr}_{0.2}\text{Ti}_{0.8}\text{O}_3$  surface layer. This evidence points to a strong chemical component to a process believed to be purely physical and has major implications for understanding ferroelectric materials, making ferroelectric devices, and interpreting local ferroelectric switching.



**KEYWORDS:** ferroelectrics, screening, chemical phenomena, ionic motion, atomic force microscopy, time-of-flight secondary ion mass spectrometry

## INTRODUCTION

Polarization switching in ferroelectric materials underpins a broad gamut of applications ranging from random access memory,<sup>1</sup> tunneling barriers,<sup>2–4</sup> data storage,<sup>5</sup> and ferroelectric ceramics.<sup>6</sup> Classically, polarization switches due to a coexistence of energetically equivalent crystallographic states can be altered with an external electric field. To stabilize single-domain state, charge discontinuity at surfaces and interfaces requires compensation, or screening, to avoid long-range electrostatic fields that destabilize the ferroelectric phase. Therefore, in materials and applications relying on polarization switching, a chemical change, reconfiguration of screening charges, also needs to be taken into account.

In a simple picture of a metal–ferroelectric interface, the screening charge comes from the conduction band of the metal. The difference in the location of screening charge and polarization-bound charge leads to convoluted behavior, described by the effective dielectric dead layer approximation. Screening at surfaces and interfaces is more complex, can be induced by either semiconductor-like band bending<sup>7,8</sup> or adsorption of ionic species,<sup>9–17</sup> and can also be supported by electrostatic energy reduction due to domain structure reorganization. The effect of screening charge dynamics on polarization screening has been described and was shown to

produce unusual phenomena such as chaos, as well as fractal domain formation.<sup>18–20</sup> In all cases, polarization screening is assumed to be chemically inert, leaving the composition of ferroelectric materials intact.

However, analysis of extant ferroelectric phenomena suggests higher complexity. It is well-known that multiple polarization switching cycles can accumulate damage at interfaces, dubbed “ferroelectric fatigue”. Typically, tens or hundreds of thousands of switching events are required, and the exact mechanisms remain controversial.<sup>21,22</sup> Furthermore, polarization-dependent photovoltaic effects in perovskites<sup>23,24</sup> and built-in potentials in compositionally graded ferroelectric thin films<sup>25</sup> suggest that even under optimal screening conditions, a considerable electric field remains in the material. Thus, switching is associated with high fields, which can chemically alter material composition.

In this work, we utilize time-of-flight secondary ion mass spectrometry (ToF-SIMS) combined with atomic force microscopy (AFM) to explore the structure property interplay of ferroelectric films during switching. Using this multimodal

Received: July 31, 2018

Accepted: October 15, 2018

Published: October 15, 2018

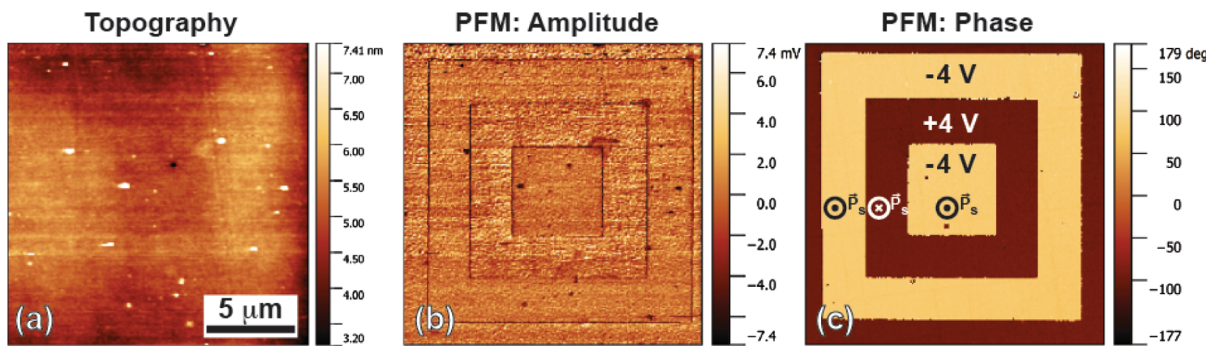


**Figure 1.** PFM measurements of the piezoresponse in the locally switched regions of a PZT thin film. (a) Topography, (b) PFM amplitude signal, and (c) PFM phase signal.

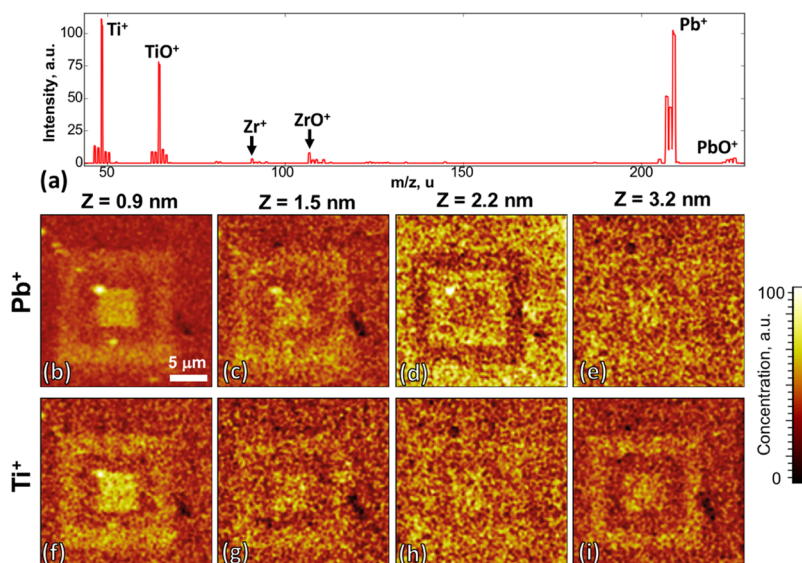


**Figure 2.** ToF-SIMS in the ferroelectrically switched region. (a) Averaged mass spectrum and (b–i) ToF-SIMS chemical maps of spatial distribution of base elements at different depths. (b–e)  $\text{Pb}^+$  and (f–i)  $\text{Ti}^+$  ions at (b,f) 0.9 nm; (c,g) 1.5 nm; (d,h) 2.2 nm; and (e,i) 3.2 nm of the depth, respectively.

chemical imaging approach, we demonstrate that local ferroelectric switching by the AFM tip significantly alters the chemical composition in the top 3 nm of the ferroelectric film. Specifically, we observe the formation of a double layer, or a concentration wave, of lead ions at the vicinity of the freshly polled region in a  $\text{PbZr}_{0.2}\text{Ti}_{0.8}\text{O}_3$  thin film. This chemical phenomenon is reversible with the bias of opposite polarity or spontaneous polarization direction. To model this behavior, we implemented numerical simulations of cations driven by an external electric field in terms of a drift diffusion model, which qualitatively demonstrated similar ion distribution near the surface of a polled ferroelectric film. This work highlights the importance of chemical phenomena in understanding the physical process of the ferroic response.

## EXPERIMENTS AND RESULTS

We used 100 nm thick ferroelectric lead zirconate titanate  $\text{PbZr}_{0.2}\text{Ti}_{0.8}\text{O}_3$  (PZT) on a 30 nm  $\text{SrRuO}_3$  bottom electrode. Experiments have been carried out using TOF-SIMS NSC (IONTOF, Germany), a combinatorial ToF-SIMS AFM in an ultrahigh vacuum chamber with pressure  $5 \times 10^{-9}$  mbar or better. An AFM tip has been used to locally switch polarization reversal by application of a dc voltage of  $\pm 4$  V, and piezoresponse force microscopy (PFM) mode has been further used to image the resulted domain structure. In the PFM mode, ac voltage with amplitude 0.5 V and frequency 300 kHz

was applied to the tip and signals of amplitude and phase of piezoresponse were measured. ToF-SIMS was used to study local chemical composition in the thin surface layer of switched PZT. Measurements were run in positive ion detection mode with the  $\text{Bi}_3^+$  primary ion beam focused down to 120 nm. More details about experimental conditions can be found in the Supporting Information, Section 1.

The experiments were performed in four steps: (1) the PZT surface was cleaned using an  $\text{O}_2$  sputter gun. Previous work has shown that sputtering with  $\text{O}_2$  is an effective way to clean and thin ferroelectric thin films while preserving their ferroelectric properties.<sup>26</sup> (2) Cleaned areas were switched using a biased AFM tip and subsequently imaged by PFM. (3) Chemical changes of the surface and the bulk of the switched regions were analyzed by ToF-SIMS using a  $\text{Bi}_3^+$  liquid metal ion gun and a time-of-flight mass detector. (4) The depth of the sputtered crater after ToF-SIMS measurements was measured by contact mode AFM. The cleaning step was essential to reveal chemical changes associated with ferroelectric phenomena and not altered by surface contamination, which can affect the chemistry of the sample due to electric field application.<sup>27</sup>

Local polarization switching was induced by a conductive AFM tip with an applied dc bias of  $\pm 4$  V. PZT was switched by scanning a square regions (Figure 1a) from 5 to 15  $\mu\text{m}$  (details of the switching procedure can be found in Section 1 of the Supporting Information) with a characteristic nested domain pattern as shown in Figure 1b,c. The outermost 15  $\mu\text{m}$  square and the innermost 5  $\mu\text{m}$  square have reversed spontaneous polarization (directed upwards), whereas the

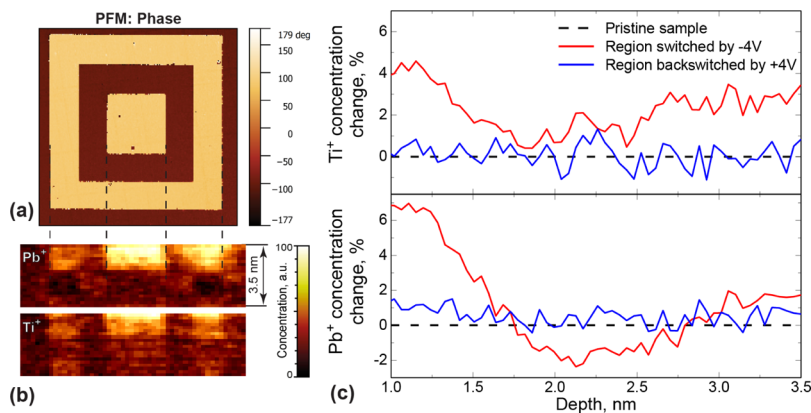


**Figure 3.** Local chemical changes in the bulk of PZT film, induced by local polarization switching. (a) PFM phase of polled regions; (b) corresponding ToF-SIMS X-Z map of  $\text{Pb}^+$  and  $\text{Ti}^+$ ; (c) depth profiles of local concentration changes with respect to the pristine sample of  $\text{Ti}^+$  (top plot) and  $\text{Pb}^+$  (bottom plot) within the outer square switched by negative bias (red line) and the middle square back-switched by positive bias (blue line).

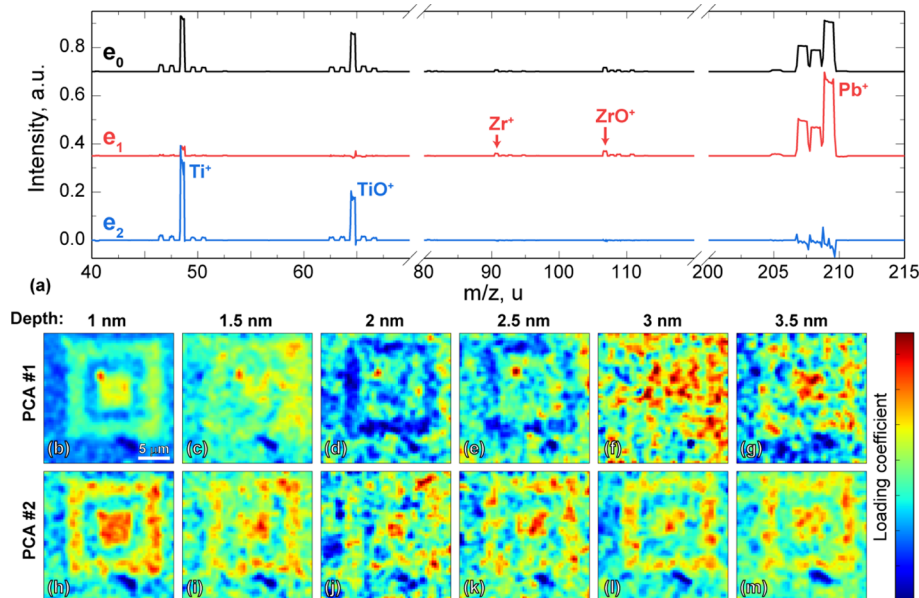


**Figure 4.** Results of PCA on the ToF-SIMS data. (a) Averaged mass spectrum  $e_0$  and first two eigenvectors. (b–m) Corresponding maps of loading coefficients at different depths (as labeled).

middle  $10 \mu\text{m}$  area was switched back to the initial, downward direction of spontaneous polarization. All produced domain structures were found to be stable—no changes were observed for at least 24 h.

ToF-SIMS studies were performed inside the polled region. The time to switch between AFM and ToF-SIMS hardware did not exceed 10 min, and the sample remained in the chamber with base pressure unaffected. In ToF-SIMS, the switched area was scanned multiple times with a focused  $\text{Bi}_3^+$  ion gun. This allowed  $\sim 120 \text{ nm}$  lateral and sub-nanometer depth resolution. The AFM analysis of the sputtered crater ([Supporting Information](#), Figure S1) was used to calibrate the chemical data depth and reconstruct local chemical changes in the PZT surface layer.

ToF-SIMS data are hyperspectral, where a mass spectrum is measured at each spatial pixel in  $x$ ,  $y$ , and  $z$  directions. Averaged mass spectra over the whole data set clearly shows the base PZT elements  $\text{Pb}^+$ ,  $\text{Zr}^+$ , and  $\text{Ti}^+$ , as well as their oxides  $\text{PbO}^+$ ,  $\text{ZrO}^+$ , and  $\text{TiO}^+$  ([Figure 2a](#)). Distribution of the peak area as a function of spatial location allowed us to characterize local chemical changes in the studied area (three-dimensional data set of all identified peaks can be found in the [Supporting Information](#), Figure S2). To simplify the data analysis and to understand the underlying chemical changes

associated with reversible polarization switching, we will focus our analysis on the most pronounced peaks— $\text{Pb}^+$  and  $\text{Ti}^+$  ([Figure 2b–i](#)).

All surface measurements revealed an increase in the concentration of base elements in the scanned regions ([Supporting Information](#), Figure S3) as well as a significant amount of  $\text{Si}^+$  ([Supporting Information](#), Figure S4). The presence of  $\text{Si}^+$  is due to the surface contamination by silicone oils, which originates from the polydimethyl siloxane gel boxes, used for tip storage.<sup>28,29</sup> This contamination affected only a thin top layer of the material ( $\sim 1 \text{ nm}$ ), which was excluded from data analysis.  $\text{Si}$  concentration was found to be independent of domain polarity and hence is not expected to affect the domain-specific phenomena.

Furthermore, the concentration of  $\text{Pb}^+$  and  $\text{Ti}^+$  clearly correlates with spontaneous polarization direction ([Figures 2b–i](#) and [3](#)) deeper in the film. Specifically, both elements are more concentrated near the surface with upward polarization direction, or polled by a negative bias ([Figure 2b,c,f,g](#)). However, at a depth of  $\sim 2.2 \text{ nm}$ ,  $\text{Pb}^+$  contrast inverts, with concentration decreasing in the negatively polled regions ([Figure 2d](#)), whereas  $\text{Ti}^+$  distribution at the same depth is almost uniform. Notably, the back-switched region at the  $10 \mu\text{m}$  square, with downward polarization, did not reveal any chemical changes with respect to the pristine sample at all depths. PFM imaging after ToF-

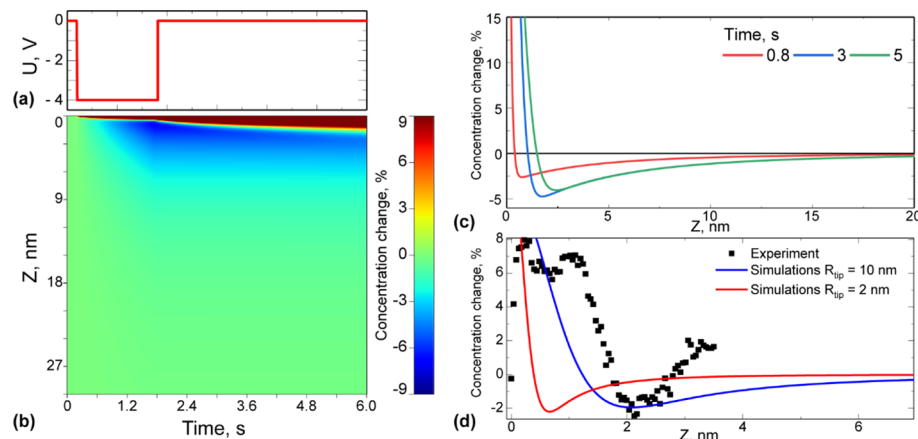


**Figure 5.** Drift diffusion simulations of the ionic motion induced by the electric field of a biased AFM tip. (a) Pulse of the applied bias, used in simulations; (b) map of local cation concentration change induced by an AFM tip bias in coordinates of time and depth; and (c,d) depth profiles of the local change in concentration as a function of time (c) and tip radius (d).

SIMS characterization revealed that the domain structure has been almost completely erased, which may be due to interaction with ion beams or removal of the top screening layer.

ToF-SIMS data, represented as a depth profile averaged over switched regions and normalized to the depth profile of the pristine sample, are shown in Figure 3c. Two regions are presented: (1) an outer 15 μm square region with polarization reversed (upward) with respect to the pristine sample shown by a red line and (2) a middle 10 μm back-switched region shown by a blue line. The concentration of Ti<sup>+</sup> and Pb<sup>+</sup> inside the back-switched region was found to be identical to the pristine sample. In the switched region, the concentration for both elements increases near the surface. We report a 7 and 4% increase in concentration for Pb<sup>+</sup> and Ti<sup>+</sup>, respectively. At about 1.7 nm into the sample, the concentration of both elements decreases to the value of the pristine sample. The decreasing trend continues for Pb<sup>+</sup>, reaching its minimum of -2% at a depth of 2.2 nm. Simultaneously, Ti<sup>+</sup> showed a slight increase at a depth of about 3 nm. The analysis of the Pb<sup>+</sup> depth profiles revealed the formation of a double layer, or a concentration wave, with a higher concentration in the top layers (15 μC/cm<sup>2</sup> or ~19% of the pristine sample) and depletion on the bottom (-6.3 μC/cm<sup>2</sup> or ~8.5% of the pristine sample).

To reveal global chemical changes in the sample across all possible elements, molecules, and functional groups, we used principal component analysis (PCA) on the multidimensional ToF-SIMS data.<sup>30–32</sup> In PCA mass spectrum,  $X_i$  in each spatial point  $i$  is represented as a sum of averaged mass spectra  $e_0$  and a linear combination of the orthogonal eigenvectors  $e_j$  with loading coefficients  $A_{ij}$ . The eigenvectors are sorted in descending order by variance. Thus, local changes in each point with respect to averaged mass spectrum can be characterized by a few first eigenvectors  $e_j$  and corresponding loading maps of the coefficients  $A_{ij}$ .

PCA of the chemical data collected from the switched PZT region showed that the whole data set can be characterized by only two eigenvectors (Figure 4a), as the third eigenvector (Supporting Information, Figure S5a) showed only changes in the peak shape (Figure S5b). Analysis of the eigenvectors revealed that the first eigenvector  $e_1$  is the change in Zr<sup>+</sup>, ZrO<sup>+</sup>, and Pb<sup>+</sup> peaks with their isotopes, whereas the second eigenvector  $e_2$  contains only peaks of Ti<sup>+</sup> and TiO<sup>+</sup>. PCA loading maps (Figure 4b) demonstrate the same trends as concentrations of Pb<sup>+</sup> and Ti<sup>+</sup>, respectively, which allows us to make a conclusion that Zr<sup>+</sup> and ZrO<sup>+</sup> concentrations demonstrate similar behavior to Pb<sup>+</sup>. Similarly, TiO<sup>+</sup> shows the same trend as Ti<sup>+</sup>.

Summarizing, local ferroelectric switching by a biased AFM tip induces ion migration in the top 3 nm layer of PZT. Changes can be only found inside the regions where the polarization was switched with respect to the pristine sample. These changes lead to formation of a Pb<sup>+</sup> concentration wave, with an induced charge of about 8–19%

of the pristine sample. At the same time, the back-switched region does not show any changes with respect to the pristine sample, which demonstrates reversibility of the induced chemical phenomena. Such results are in good agreement with the conception of dead layer, reducing the depolarization field on the film interfaces.<sup>33,34</sup>

These chemical changes are likely to be caused by depolarization field, which in turn is caused by the unscreened charges on the freshly polished polar faces of the ferroelectric film. Commonly, screening is provided by charge redistribution in external electrodes; however, with AFM tip induced switching, there is no top electrode. In this case, observed phenomena are likely caused by the redistribution of the point defects in the vicinity of the PZT surface. It is known that most common defects in PZT are represented by oxygen and lead vacancies,<sup>35</sup> with oxygen vacancies having much higher values of mobility.<sup>36</sup> High values of the depolarization electric field in the surface vicinity lead to defect redistribution with creation of the screening layer, reducing the total electric field. Low mobility of lead ions in this case limits redistribution depth.

This process can be simulated in terms of a drift diffusion model. In the simple one-dimensional case, the cation concentration  $c$  along the  $z$ -axis will be defined by eq 1

$$\frac{\partial c}{\partial t} = D \frac{\partial^2 c}{\partial z^2} + \frac{\partial}{\partial z}(cv) \quad (1)$$

where  $D$  is the diffusion coefficient and  $v$  is the drift speed. Drift speed  $v$  can be directly proportional to the electric field produced by the biased AFM tip. Here, we consider a spherical tip apex to calculate the drift speed, given by eq 2

$$v_x(z, t) = \mu_{\text{ion}} E_{\text{tip}}(z, t) = \mu_{\text{ion}} \frac{U_{\text{tip}}(t) R_{\text{tip}}}{(z + R_{\text{tip}})^2} \quad (2)$$

where  $\mu_{\text{ion}}$  is the effective ion mobility,  $R_{\text{tip}}$  is the tip radius of curvature, and  $U_{\text{tip}}$  is the bias applied to the tip. Ion mobility, in turn, can be related with diffusion coefficient using Einstein relation in eq 3

$$D = \frac{\mu_{\text{ion}} k_B T}{q} \quad (3)$$

where  $k_B$  is the Boltzmann's constant,  $T$  is the temperature, and  $q$  is the ion charge. Using eqs 1–3, we performed numerical simulations of the ionic motion induced by the electric field of a biased AFM tip (Figure 5).

Initially, concentration was uniformly distributed over the model  $c(z, t)|_{t=0} = c_0$  and the boundary conditions excluded ionic flux through the edges. Electrical bias was simulated by a pulse with an amplitude of 4 V and a duration of 1.8 s (Figure 5a). Calculations were performed in a COMSOL Multiphysics finite element environment

and allowed us to observe local concentration change near the sample surface during application of the electric field and its relaxation after switching the field off (Figure 5b).

As expected, simulations demonstrated the formation of a concentration wave near the surface (Figure 5c); however, the shape of the profile differed from the experimentally observed data (Figure 5d). We used a tip radius of about 10 nm, similar to what was used in the experiment. Concentration changed down to about 5 nm into the bulk, larger than the experimentally observed 2 nm. Simulations with a smaller tip radius showed wave localization near the sample surface, which also disagrees with the experiment. These disagreements show that the used simple model cannot completely describe this system, as electrostatics, chemistry, screening, and depolarization are not considered. A more precise model should consider electromigration as a self-consistent problem, where ionic motion changes distribution of the electric fields and vice versa. In this case, simulation should include a Poisson equation and mobility of the charge carriers. Such advanced simulation is beyond the scope of the current work and will be published elsewhere. However, a simple drift diffusional model allowed to qualitatively show behavior similar to experiment and adequately represents the formation of a concentration wave in the switched PZT. Values for the diffusion coefficient corresponding to best agreement with experiment were found to be around  $D = 3.2 \times 10^{-19} \text{ m}^2/\text{s}$  and corresponding lead ion mobility  $\mu_{\text{Pb}} = 2.5 \times 10^{-16} \text{ m}^2/(\text{V}\cdot\text{s})$ .

## CONCLUSIONS

In conclusion, we utilized a multimodal chemical imaging platform that combines AFM with ToF-SIMS in ultrahigh vacuum to study the chemistry of local ferroelectric switching. Our data showed significant changes in the local concentration of the base elements in the top 3 nm thick surface layer of a lead zirconate titanate thin film, after switching by an AFM tip. Lead ions formed a double layer, or a concentration wave within 2 nm from the sample surface. These chemical changes were found to be reversible and correlated with the direction of spontaneous polarization. A drift diffusion model was utilized to qualitatively explain the chemical changes. The simulation supplemented the experiment and allowed us to attribute the observed phenomenon to cation motion induced by the superposition of electric fields near the surface of freshly switched ferroelectric film. We believe that this insight will enhance the fundamental understanding of ferroelectric phenomena and aid in the practical application of ferroelectric materials in devices. For instance, explored chemical phenomena can be used to explain ferroelectric fatigue.

## ASSOCIATED CONTENT

### Supporting Information

The Supporting Information is available free of charge on the ACS Publications website at DOI: [10.1021/acsami.8b13034](https://doi.org/10.1021/acsami.8b13034).

AFM and ToF-SIMS experiments, as well as additional images on ToF-SIMS imaging, data analysis, and depth calibration ([PDF](#))

## AUTHOR INFORMATION

### Corresponding Authors

\*E-mail: [ievlevav@ornl.gov](mailto:ievlevav@ornl.gov) (A.V.I.).

\*E-mail: [ovchinnikovo@ornl.gov](mailto:ovchinnikovo@ornl.gov) (O.S.O.).

### ORCID

Anton V. Ievlev: [0000-0003-3645-0508](https://orcid.org/0000-0003-3645-0508)

Lane W. Martin: [0000-0003-1889-2513](https://orcid.org/0000-0003-1889-2513)

Alex Belianinov: [0000-0002-3975-4112](https://orcid.org/0000-0002-3975-4112)

Sergei V. Kalinin: [0000-0001-5354-6152](https://orcid.org/0000-0001-5354-6152)

Olga S. Ovchinnikova: [0000-0001-8935-2309](https://orcid.org/0000-0001-8935-2309)

### Notes

The authors declare no competing financial interest.

## ACKNOWLEDGMENTS

This research was conducted at the Center for Nanophase Materials Sciences, which is a DOE Office of Science User Facility, and using instrumentation within ORNL's Materials Characterization Core provided by UT-Battelle, LLC, under contract no. DE-AC05-00OR22725 with the U.S. Department of Energy. AVI and OSO were supported by the Laboratory Directed Research and Development Program of Oak Ridge National Laboratory. This manuscript has been authored by UT-Battelle, LLC, under contract no. DE-AC0500OR22725 with the U.S. Department of Energy. The United States Government retains and the publisher, by accepting the article for publication, acknowledges that the United States Government retains a nonexclusive, paid-up, irrevocable, worldwide license to publish or reproduce the published form of this manuscript, or allow others to do so, for the United States Government purposes. The Department of Energy will provide public access to these results of federally sponsored research in accordance with the DOE Public Access Plan (<http://energy.gov/downloads/doe-public-access-plan>).

## REFERENCES

- (1) Scott, J. F.; Paz de Araujo, C. A. Ferroelectric Memories. *Science* **1989**, *246*, 1400–1405.
- (2) Gruverman, A.; Wu, D.; Lu, H.; Wang, Y.; Jang, H. W.; Folkman, C. M.; Zhuravlev, M. Y.; Felker, D.; Rzchowski, M.; Eom, C.-B.; Tsymbal, E. Y. Tunneling Electroresistance Effect in Ferroelectric Tunnel Junctions at the Nanoscale. *Nano Lett.* **2009**, *9*, 3539–3543.
- (3) Tsymbal, E. Y.; Kohlstedt, H. APPLIED PHYSICS: Tunneling Across a Ferroelectric. *Science* **2006**, *313*, 181–183.
- (4) Maksymovich, P.; Jesse, S.; Yu, P.; Ramesh, R.; Baddorf, A. P.; Kalinin, S. V. Polarization Control of Electron Tunneling into Ferroelectric Surfaces. *Science* **2009**, *324*, 1421–1425.
- (5) Ahn, C. H.; Tybille, T.; Antognazza, L.; Char, K.; Hammond, R. H.; Beasley, M. R.; Fischer, Ø.; Triscone, J. M. Local, Nonvolatile Electronic Writing of Epitaxial Pb(Zr<sub>0.52</sub>Ti<sub>0.48</sub>)O<sub>3</sub>/SrRuO<sub>3</sub> Heterostructures. *Science* **1997**, *276*, 1100–1103.
- (6) Setter, N.; Damjanovic, D.; Eng, L.; Fox, G.; Gevorgian, S.; Hong, S.; Kingon, A.; Kohlstedt, H.; Park, N. Y.; Stephenson, G. B.; Stolitchnov, I.; Tagantsev, A. K.; Taylor, D. V.; Yamada, T.; Streiffer, S. Ferroelectric thin films: Review of materials, properties, and applications. *J. Appl. Phys.* **2006**, *100*, 051606.
- (7) Fridkin, V. M. *Ferroelectric Semiconductors*; Springer: New York, 1980.
- (8) Vul, B. M.; Guro, G. M.; Ivanchik, I. I. Encountering domains in ferroelectrics. *Ferroelectrics* **1973**, *6*, 29–31.
- (9) Highland, M. J.; Fister, T. T.; Fong, D. D.; Fuoss, P. H.; Thompson, C.; Eastman, J. A.; Streiffer, S. K.; Stephenson, G. B. Equilibrium Polarization of Ultrathin PbTiO<sub>3</sub> with Surface Compensation Controlled by Oxygen Partial Pressure. *Phys. Rev. Lett.* **2011**, *107*, 187602.
- (10) Highland, M. J.; Fister, T. T.; Richard, M.-I.; Fong, D. D.; Fuoss, P. H.; Thompson, C.; Eastman, J. A.; Streiffer, S. K.; Stephenson, G. B. Polarization Switching without Domain Formation at the Intrinsic Coercive Field in Ultrathin Ferroelectric PbTiO<sub>3</sub>. *Phys. Rev. Lett.* **2010**, *105*, 167601.
- (11) Wang, R. V.; Fong, D. D.; Jiang, F.; Highland, M. J.; Fuoss, P. H.; Thompson, C.; Kolpak, A. M.; Eastman, J. A.; Streiffer, S. K.; Rappe, A. M.; Stephenson, G. B. Reversible Chemical Switching of a Ferroelectric Film. *Phys. Rev. Lett.* **2009**, *102*, 047601.
- (12) Fong, D. D.; Kolpak, A. M.; Eastman, J. A.; Streiffer, S. K.; Fuoss, P. H.; Stephenson, G. B.; Thompson, C.; Kim, D. M.; Choi, K.

- J.; Eom, C. B.; Grinberg, I.; Rappe, A. M. Stabilization of monodomain polarization in ultrathin PbTiO<sub>3</sub> films. *Phys. Rev. Lett.* **2006**, *96*, 127601.
- (13) Kalinin, S. V.; Johnson, C. Y.; Bonnell, D. A. Domain polarity and temperature induced potential inversion on the BaTiO<sub>3</sub>(100) surface. *J. Appl. Phys.* **2002**, *91*, 3816–3823.
- (14) Kalinin, S. V.; Bonnell, D. A. Effect of phase transition on the surface potential of the BaTiO<sub>3</sub> (100) surface by variable temperature scanning surface potential microscopy. *J. Appl. Phys.* **2000**, *87*, 3950–3957.
- (15) Kalinin, S. V.; Bonnell, D. A. Local potential and polarization screening on ferroelectric surfaces. *Phys. Rev. B: Condens. Matter Mater. Phys.* **2001**, *63*, 125411.
- (16) Shur, V. Y.; Ievlev, A. V.; Nikolaeva, E. V.; Shishkin, E. I.; Neradovskiy, M. M. Influence of adsorbed surface layer on domain growth in the field produced by conductive tip of scanning probe microscope in lithium niobate. *J. Appl. Phys.* **2011**, *110*, 052017.
- (17) Ievlev, A. V.; Morozovska, A. N.; Shur, V. Y.; Kalinin, S. V. Humidity effects on tip-induced polarization switching in lithium niobate. *Appl. Phys. Lett.* **2014**, *104*, 092908.
- (18) Ievlev, A. V.; Alikin, D. O.; Morozovska, A. N.; Varenyk, O. V.; Eliseev, E. A.; Kholkin, A. L.; Shur, V. Y.; Kalinin, S. V. Symmetry Breaking and Electrical Frustration during Tip-Induced Polarization Switching in the Nonpolar Cut of Lithium Niobate Single Crystals. *ACS Nano* **2015**, *9*, 769–777.
- (19) Ievlev, A. V.; Jesse, S.; Morozovska, A. N.; Strelcov, E.; Eliseev, E. A.; Pershin, Y. V.; Kumar, A.; Shur, V. Y.; Kalinin, S. V. Intermittency, quasiperiodicity and chaos in probe-induced ferroelectric domain switching. *Nat. Phys.* **2014**, *10*, 59–66.
- (20) Ievlev, A. V.; Morozovska, A. N.; Eliseev, E. A.; Shur, V. Y.; Kalinin, S. V. Ionic field effect and memristive phenomena in single-point ferroelectric domain switching. *Nat. Commun.* **2014**, *5*, 5545.
- (21) Scott, J. F.; Dawber, M. Oxygen-vacancy ordering as a fatigue mechanism in perovskite ferroelectrics. *Appl. Phys. Lett.* **2000**, *76*, 3801–3803.
- (22) Tagantsev, A. K.; Stolichnov, I.; Colla, E. L.; Setter, N. Polarization fatigue in ferroelectric films: Basic experimental findings, phenomenological scenarios, and microscopic features. *J. Appl. Phys.* **2001**, *90*, 1387–1402.
- (23) Kalinin, S. V.; Gruverman, A.; Bonnell, D. A. Quantitative analysis of nanoscale switching in SrBi<sub>2</sub>Ta<sub>2</sub>O<sub>9</sub> thin films by piezoresponse force microscopy. *Appl. Phys. Lett.* **2004**, *85*, 795–797.
- (24) Haussmann, A.; Milde, P.; Erler, C.; Eng, L. M. Ferroelectric Lithography: Bottom-up Assembly and Electrical Performance of a Single Metallic Nanowire. *Nano Lett.* **2009**, *9*, 763–768.
- (25) Agar, J. C.; Damodaran, A. R.; Velarde, G. A.; Pandya, S.; Mangalam, R. V. K.; Martin, L. W. Complex Evolution of Built-in Potential in Compositionally-Graded PbZr<sub>1-x</sub>Ti<sub>x</sub>O<sub>3</sub> Thin Films. *ACS Nano* **2015**, *9*, 7332–7342.
- (26) Ievlev, A. V.; Chyasnichiyus, M.; Leonard, D. N.; Agar, J. C.; Velarde, G. A.; Martin, L. W.; Kalinin, S. V.; Maksymovych, P.; Ovchinnikova, O. S. Subtractive fabrication of ferroelectric thin films with precisely controlled thickness. *Nanotechnology* **2018**, *29*, 155302.
- (27) Ievlev, A. V.; Maksymovych, P.; Trassin, M.; Seidel, J.; Ramesh, R.; Kalinin, S. V.; Ovchinnikova, O. S. Chemical State Evolution in Ferroelectric Films during Tip-Induced Polarization and Electroresistive Switching. *ACS Appl. Mater. Interfaces* **2016**, *8*, 29588–29593.
- (28) Lo, Y.-S.; Huefner, N. D.; Chan, W. S.; Dryden, P.; Hagenhoff, B.; Beebe, T. P. Organic and inorganic contamination on commercial AFM cantilevers. *Langmuir* **1999**, *15*, 6522–6526.
- (29) Ievlev, A. V.; Brown, C.; Burch, M. J.; Agar, J. C.; Velarde, G. A.; Martin, L. W.; Maksymovych, P.; Kalinin, S. V.; Ovchinnikova, O. S. Chemical Phenomena of Atomic Force Microscopy Scanning. *Anal. Chem.* **2018**, *90*, 3475–3481.
- (30) Jesse, S.; Kalinin, S. V. Principal component and spatial correlation analysis of spectroscopic-imaging data in scanning probe microscopy. *Nanotechnology* **2009**, *20*, 085714.
- (31) Biesinger, M. C.; Paepegaey, P.-Y.; McIntyre, N. S.; Harbottle, R. R.; Petersen, N. O. Principal component analysis of TOF-SIMS images of organic monolayers. *Anal. Chem.* **2002**, *74*, 5711–5716.
- (32) Ievlev, A. V.; Belianinov, A.; Jesse, S.; Allison, D. P.; Doktycz, M. J.; Rettner, S. T.; Kalinin, S. V.; Ovchinnikova, O. S. Automated Interpretation and Extraction of Topographic Information from Time of Flight Secondary Ion Mass Spectrometry Data. *Sci. Rep.* **2017**, *7*, 17099.
- (33) Bratkovsky, A. M.; Levanyuk, A. P. Abrupt Appearance of the Domain Pattern and Fatigue of Thin Ferroelectric Films. *Phys. Rev. Lett.* **2000**, *84*, 3177–3180.
- (34) Bratkovsky, A. M.; Levanyuk, A. P. Continuous Theory of Ferroelectric States in Ultrathin Films with Real Electrodes. *J. Comput. Theor. Nanosci.* **2009**, *6*, 465–489.
- (35) Boukamp, B.; Pham, M.; Blank, D.; Bouwmeester, H. Ionic and electronic conductivity in lead-zirconate-titanate (PZT). *Solid State Ionics* **2004**, *170*, 239–254.
- (36) Raymond, M. V.; Smyth, D. M. Defects and charge transport in perovskite ferroelectrics. *J. Phys. Chem. Solids* **1996**, *57*, 1507–1511.